

1           **Impacts of Three Gorges Dam’s operation on spatial-temporal**  
2           **patterns of tide-river dynamics in the Yangtze River estuary, China**

3           Huayang Cai<sup>1,2,3,4</sup>, Xianyi Zhang<sup>1,2,3</sup>, Leicheng Guo<sup>4</sup>, Min Zhang<sup>5,\*</sup>, Feng Liu<sup>1,2,3</sup>,  
4           Qingshu Yang<sup>1,2,3</sup>

5  
6           1. *Institute of Estuarine and Coastal Research, School of Marine Engineering and*  
7           *Technology, Sun Yat-sen University, Guangzhou, China*

8           2. *Guangdong Provincial Engineering Research Center of Coasts, Islands and Reefs,*  
9           *Guangzhou, China*

10          3. *Southern Marine Science and Engineering Guangdong Laboratory (Zhuhai),*  
11          *Zhuhai, China*

12          4. *State Key Laboratory of Estuarine and Coastal Research, East China Normal*  
13          *University, Shanghai, China*

14          5. *Shanghai Normal University, School of Environmental and Geographical Sciences,*  
15          *Shanghai, China*

16          **Corresponding author:** Min Zhang

17          **Corresponding author’s E-mail:** zhangmin@shnu.edu.cn

18  
19          **Key points**

20          1. Impacts of TGD operation on tide-river dynamics are quantified using an analytical  
21          model.

22          2. The strongest impacts occurred during autumn and winter due to the seasonal  
23          freshwater regulation by TGD.

24          3. The alteration of tide-river dynamics may exert considerable impacts on sustainable  
25          water resource management in dam-controlled estuaries.

26

27

28

29

30 **Abstract**

31 The Three Gorges Dam (TGD), located in the mainstream of the Yangtze River, is the  
32 world's largest hydroelectric station in terms of installed power capacity. It was  
33 demonstrated that the TGD had caused considerable modifications in the downstream  
34 freshwater discharge due to its seasonal operation mode of multiple utilisation for flood  
35 control, irrigation, and power generation. To understand the impacts of the freshwater  
36 regulation of TGD, an analytical model is adopted to explore how the operation of TGD  
37 may affect the spatial-temporal patterns of tide-river dynamics in the Yangtze River  
38 estuary. We evaluated the effect of TGD by comparing the changes in major tide-river  
39 dynamics in the post-TGD period (2003–2014) with those in the pre-TGD period  
40 (1979–1984). The results indicate that the strongest impacts occurred during the autumn  
41 and winter, corresponding to a substantial reduction in freshwater discharge during the  
42 wet-to-dry transition period and slightly increased discharge during the dry season. The  
43 underlying mechanism leading to changes in the tide-river dynamics lies in the  
44 alteration of freshwater discharge, while the impact of geometric change is minimal.  
45 Overall, the results suggest that the spatial-temporal pattern of tide-river dynamics is  
46 sensible to the freshwater regulation of the TGD, so that the ecosystem function of the  
47 estuary may undergo profound disturbances. The results obtained from this study can  
48 be used to set scientific guidelines for water resource management (e.g. navigation,  
49 flood control, salt intrusion) in dam-controlled estuarine systems.

50 **Key words:** seasonal freshwater regulation, Three Gorges Dam, analytical model, tide-  
51 river dynamics, Yangtze River estuary

52 **1. Introduction**

53 Estuaries are transition zones where river meets ocean (Savenije, 2012). Tide-river  
54 interactions, a result of both hydrologic drivers and geomorphic constraints, are highly  
55 dynamic in estuaries (Buschman et al., 2009; Sassi and Hoitink, 2013; Guo et al., 2015;  
56 Cai et al., 2016; Hoitink and Jay, 2016; Hoitink et al., 2017; Du et al., 2018). In natural  
57 conditions, they usually experience a wide range of temporal variations, in timescale  
58 ranging from a fortnight to season (e.g. Zhang et al., 2018). Human intervention, such  
59 as dam construction in the upstream parts of a river and the growing number of water  
60 conservancy projects built along large rivers (such as freshwater withdrawal), have  
61 caused seasonal changes in downstream freshwater discharge delivery, leading to  
62 adjustments in the function of fluvial and estuarine hydrology (e.g. Lu et al., 2011; Mei  
63 et al., 2015; Dai et al., 2017). Consequently, it is important to understand the impacts  
64 of large-scale human intervention, such as flood control, navigation, salt intrusion, and  
65 freshwater withdrawal, which are relevant not only to tide-river dynamics and riparian  
66 ecology but also to sustainable water resource management in general.

67

68 River discharge generally fluctuates following a wet-dry cycle due to the seasonal  
69 variation of precipitation in the upstream river basin. For instance, the Yangtze River,  
70 the largest river in China in terms of mean discharge, which flows into the East China  
71 Sea, has a maximum river discharge during summer in July and a low value during  
72 winter in January, with a maximum discharge difference of approximately 38,000 m<sup>3</sup>/s  
73 (Cai et al., 2016). Similar seasonal variations are also identified in other large rivers in

74 eastern and southern Asia, such as the Mekong River in Vietnam, Ganges River in India,  
75 and Pearl River in China, under the influence of a monsoon climate. However, most  
76 large rivers have been significantly dammed at the central and upper reaches in recent  
77 decades, dramatically modifying stream hydrology and sediment delivery, resulting in  
78 changes in hydraulics and river delta development trend at the lower reaches (e.g.  
79 Räsänen et al, 2017; Rahman et al., 2018; Liu et al., 2018). Due to the fact that the  
80 response of tide-river interactions to the impacts of dams are diverse and non-uniform  
81 and that many more dams are to be built in the future, the impacts of the hydrodynamic  
82 interactions between tidal waves and seasonal river flows from natural variations and  
83 anthropogenic activities have become a common focus in international hydraulic  
84 research, especially in large tidal rivers.

85

86 The Yangtze River estuary, located near the coastal area of East China Sea, is one of the  
87 largest estuaries in Asia. In the mouth of the Yangtze River estuary, bifurcation occurs  
88 and the characteristics of tides have been broadly investigated in previous studies (e.g.  
89 Zhang et al., 2012; Lu et al., 2015; Alebregtse and Swart, 2016). However, in these  
90 studies, river influences are usually neglected. In recent years, the processes of  
91 nonlinear interactions between tidal wave and river flow in the Yangtze River estuary  
92 have received increasing attention (e.g. Guo et al., 2015; Zhang et al., 2015a, b; Cai et  
93 al., 2016; Kuang et al., 2017; Zhang et al., 2018). However, recent studies on tidal  
94 properties, such as asymmetry, changes near the mouth area, and seasonal variations in  
95 tidal wave propagation and fluvial effects over the entire 600 km of the tidal river, up

96 to the tidal limit of the Datong hydrological station, have been limited. In addition, the  
97 operation of the Three Gorges Dam (TGD), the largest dam in the world, has  
98 substantially affected the downstream river hydrology and sediment delivery. There is  
99 a variety of debate regarding the potential impacts of TGD on the downstream river  
100 morphology, hydrology, and ecology, since the underlying mechanism of the impact of  
101 the TGD is not fully understood. Specifically, the TGD operation has altered the  
102 downstream fluvial discharge and water levels on the seasonal scale, directly following  
103 the reservoir seasonal impounding and release of water volume (e.g. Chen et al., 2016;  
104 Guo et al., 2018). However, the impacts of seasonal freshwater regulation by the TGD  
105 on the spatial-temporal tide-river dynamics in the downstream estuarine area have not  
106 been systematically investigated. For example, during the dry season TGD operation  
107 increased the multi-year monthly averaged river discharge at Datong station from 9520  
108  $\text{m}^3 \cdot \text{s}^{-1}$  to 12896  $\text{m}^3 \cdot \text{s}^{-1}$  in January, while during wet season the regulation reduced the  
109 river discharge from 49900  $\text{m}^3 \cdot \text{s}^{-1}$  to 44367  $\text{m}^3 \cdot \text{s}^{-1}$  in July during the pre- and post- TGD  
110 period.

111

112 In this study, for the first time, the spatial-temporal variations in the hydrodynamic  
113 processes due to the interactions of tidal flow and fluvial discharge in the Yangtze River  
114 estuary caused by natural forcing and human intervention were studied, with specific  
115 focus on the effect of TGD seasonal regulation. Here, we adopted a well-developed  
116 analytical model proposed by Cai et al. (2014a, 2016) to investigate the spatial-temporal  
117 patterns of tide-river dynamics in the entire Yangtze River estuary and quantify the

118 impacts of the TGD operation. In the following sections, we introduce the study site of  
119 the Yangtze River estuary. This is followed by a description of the available data and  
120 analytical model of tide-river dynamics in Section 3. Subsequently, we applied the  
121 model to the Yangtze River estuary, where the TGD has operated since 2003 (Section  
122 4). In particular, we explored the alteration of the tide-river dynamics after the TGD  
123 closure and summarise the impacts of the TGD on the spatial-temporal patterns of tide-  
124 river dynamics. The impacts of channel geometry and river discharge alterations on  
125 tide-river dynamics as well as the implications for sustainable water resource  
126 management were then discussed in Section 5. Finally, some key findings were  
127 addressed in Section 6.

128

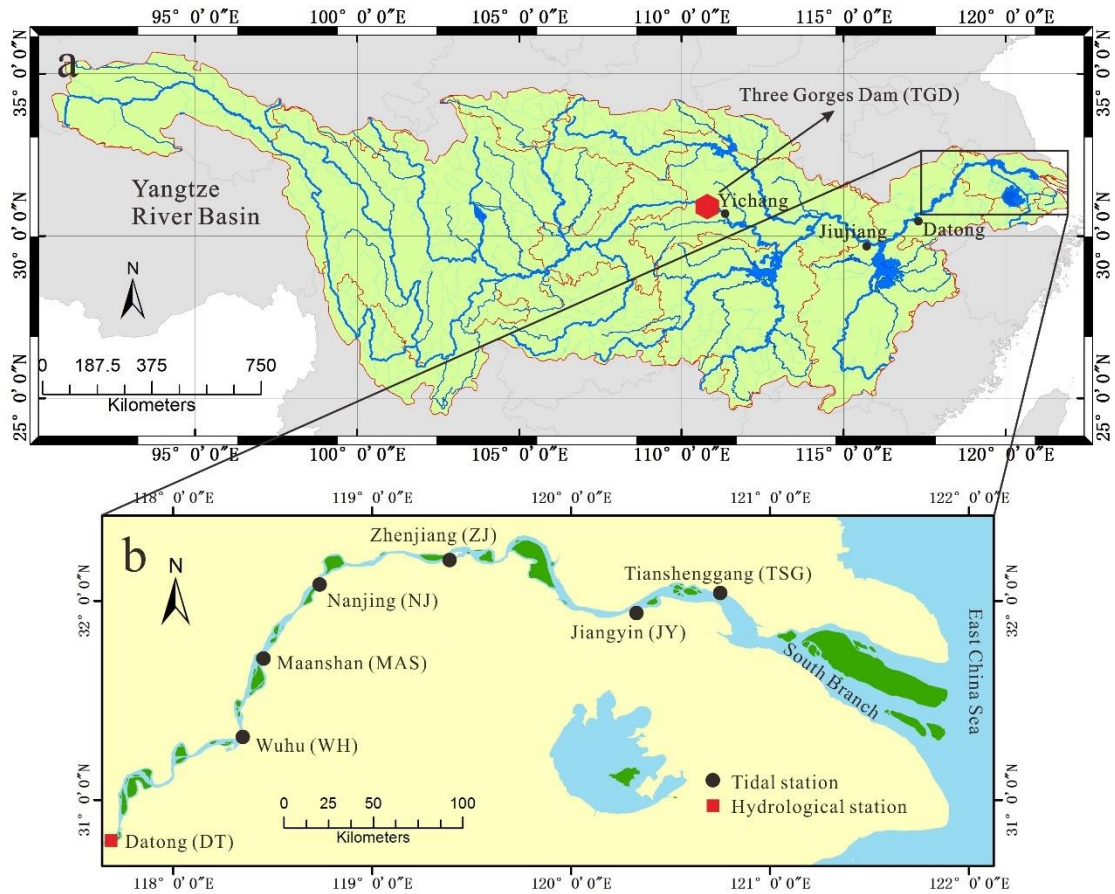
## 129 **2. Overview of the Yangtze River estuary**

130 The Yangtze River, flowing from west to east in central China, is one of the world's  
131 most important rivers due to its great economic and social relevance. It has a length of  
132 about 6300 km and a basin area of about 190,000 km<sup>2</sup> (Figure 1a). The Yangtze River  
133 basin is geographically divided into three parts, the upper, central, and lower sub-basins,  
134 and contains an estuary area with partitions at Yichang, Jiujiang, and Datong (DT),  
135 respectively (Figure 1a). Of concern in this study are the impacts of the Three Gorges  
136 Dam (TGD), the world's largest dam, on the spatial-temporal patterns of tide-river  
137 dynamics in the estuarine area. It is located about 45 km upstream of Yichang (Figure  
138 1a). The TGD project began in 2003; by 2009, when full operations began, the total  
139 water storage capacity rose up to ~40 km<sup>3</sup>, equivalent to 5% of the Yangtze's annual

140 discharge. Downstream the DT station, where the tidal limit is located, the Yangtze  
141 River estuary extends ~630 km to the seaward end of the South Branch. Wuhu (WH),  
142 Maanshan (MAS), Nanjing (NJ), Zhenjiang (ZJ), Jiangyin (JY), and Tianshenggang  
143 (TSG) are the major gauging stations along the mainstream in the seaward direction  
144 (Figure 1b). Under the control of the Asian monsoon climate, river discharges show  
145 distinct seasonal patterns. In 1979–2012, more than 70% of freshwater was discharged  
146 at DT occurred during summer (May–October).

147

148 Apart from river flows, tidal waves are also recognised as the major sources of energy  
149 for hydrodynamics in the Yangtze River estuary, which is characterised by a meso-tide  
150 with a tidal range of up to 4.6 m and a mean tidal range of ~2.7 m near the estuary  
151 mouth. According to the observation in the Gaoqiaoju tidal gauging station (1950–  
152 2012), the averaged ebb tide duration (7.5 h) is a bit longer than the averaged flood tide  
153 duration (5 h), indicating an irregular semidiurnal character (Zhang et al., 2012).



154

155 Figure 1. Maps of the Yangtze River basin (a) and Yangtze River estuary (b) with the  
 156 location of tidal gauging and hydrological stations shown with black solid circles and  
 157 red solid rectangles.

158

### 159 3. Data and Methodology

#### 160 3.1 Source of Data

161 To quantitatively investigate the relationship between freshwater discharge regulation  
 162 caused by the TGD operation and the tide-river dynamics, monthly averaged  
 163 hydrological data for both pre-TGD (1979–1984) and post-TGD (2003–2014) periods  
 164 of tidal range and water level from the above-mentioned six tidal gauging stations along  
 165 the Yangtze River estuary were collected. They were published by the Yangtze



166 Hydrology Bureau of the People's Republic of China. The monthly averaged tidal  
167 amplitude is determined by averaging the daily difference between high and low water  
168 levels and dividing by two. To correctly quantify the residual water level along the  
169 Yangtze estuary, locally measured water level at different gauging stations are corrected  
170 to the national mean sea level of Huanghai 1985.

171

## 172 **3.2 Analytical model for tide-river dynamics**

### 173 **3.2.1 Basic equations**

174 In tidal rivers, the tidally averaged water level (i.e. residual water level) depicts a steady  
175 gradient, which usually increases with freshwater discharge (e.g. Sassi and Hoitink,  
176 2013). The key to deriving the dynamics of the residual water level lies in the one-  
177 dimensional momentum equation, which can be expressed as (e.g. Savenije, 2005,  
178 2012):

$$179 \quad \frac{\partial U}{\partial t} + U \frac{\partial U}{\partial x} + g \frac{\partial Z}{\partial x} + \frac{gh}{2\rho} \frac{\partial \rho}{\partial x} + g \frac{U|U|}{K^2 h^{4/3}} = 0, \quad (1)$$

180 where  $U$  is the cross-sectional averaged velocity,  $Z$  is the free surface elevation,  $h$  is the  
181 water depth,  $g$  is the acceleration due to gravity,  $t$  is the time,  $\rho$  is the water density,  $x$  is  
182 the longitudinal coordinate directed landward, and  $K$  is the Manning-Strickler friction  
183 coefficient. It was demonstrated that in the subtidal momentum balance, the residual  
184 water level slope is primarily balanced by the residual friction term (Vignoli et al., 2003;  
185 Buschman et al., 2009; Cai et al., 2014a, for a detailed derivation, readers can refer to  
186 the Appendix A):

$$187 \quad \overline{\frac{\partial Z}{\partial x}} = -\overline{\frac{U|U|}{K^2 h^{4/3}}} \quad (2)$$

188

189 where the overbars indicate the tidal average. For a single channel with the residual  
190 water level set to 0 at the estuary mouth (i.e.  $\bar{Z} = 0$  at  $x = 0$ ), the integration of  
191 Equation (2) leads to an analytical expression for the residual water level

$$192 \quad \bar{Z}(x) = -\int_0^x \frac{\partial \bar{Z}}{\partial x} = -\int_0^x \frac{\overline{U|U|}}{K^2 h^{4/3}} . \quad (3)$$

193 To derive the analytical solutions for tide-river dynamics, we assume that the  
194 longitudinal variation of cross-sectional area  $\bar{A}$  and width  $\bar{B}$  can be described by the  
195 following exponential functions (see also Toffolon et al., 2006; Cai et al., 2014a):

$$196 \quad \bar{A} = \bar{A}_r + (\bar{A}_0 - \bar{A}_r) \exp\left(-\frac{x}{a}\right), \quad (4)$$

$$197 \quad \bar{B} = \bar{B}_r + (\bar{B}_0 - \bar{B}_r) \exp\left(-\frac{x}{b}\right), \quad (5)$$

198 where  $\bar{A}_0$  and  $\bar{B}_0$  represent the tidally averaged cross-sectional area and width at the  
199 estuary mouth, respectively,  $\bar{A}_r$  and  $\bar{B}_r$  represent the asymptotic riverine cross-  
200 sectional area and width, respectively, and  $a$  and  $b$  are the convergence lengths of the  
201 cross-sectional area and width, respectively. The advantage of these equations for  
202 approximating the shape of the estuary is that they account not only for the exponential  
203 shape in the lower part of the tidal river but also for the approximately prismatic channel  
204 in the upstream part of the tidal river. We further assume a nearly rectangular cross-  
205 section, considering a large width to depth ratio; hence, the tidally averaged depth is  
206 given by  $\bar{h} = \bar{A}/\bar{B}$  and the cross-sectional area variability can be primarily attributed  
207 to the change in depth.

### 208 **3.2.2 Analytical solution for tidal hydrodynamics**

209 It was shown by Cai et al. (2014a, b, 2016) that the tide-river dynamics is dominantly  
 210 controlled by four dimensionless parameters (see their definitions in Table 1). They  
 211 include: the dimensionless tidal amplitude  $\zeta$  (representing the boundary condition in the  
 212 seaward side), the estuary shape number  $\gamma$  (representing the cross-sectional area  
 213 convergence), the friction number  $\chi$  (representing the bottom frictional effect), and the  
 214 dimensionless river discharge  $\varphi$  (representing the impact of freshwater discharge). The  
 215 definitions of these four variables are defined in Table 1, where  $\eta$  is the tidal amplitude,  
 216  $v$  is the velocity amplitude,  $U_r$  is the river flow velocity,  $\omega$  is the tidal frequency,  $r_s =$   
 217  $B_S/\bar{B}$  is the storage width ratio between the storage width  $B_S$  and the stream width  $\bar{B}$   
 218 that accounts for the effect of storage area (i.e., tidal flats or salt marshes), and  $c_0$  is the  
 219 classical wave celerity defined as  $c_0 = \sqrt{g\bar{h}/r_s}$ .

220 Table 1. Definitions of dimensionless parameters used in the analytical model

| Local variables  | Dependent variables   |
|--|---|
| Dimensionless tidal amplitude<br>$\zeta = \eta / \bar{h}$  | Amplification number<br>$\delta = c_0 d \eta / (\eta \omega d x)$           |
| Estuary shape number<br>$\gamma = c_0 (\bar{A} - \bar{A}_r) / (\omega a \bar{A})$                  | Velocity number<br>$\mu = v / (r_s \zeta c_0) = v \bar{h} / (r_s \eta c_0)$ |
| Friction number<br>$\chi = r_s g c_0 \zeta [1 - (4\zeta / 3)^2]^{-1} / (\omega K^2 \bar{h}^{4/3})$ | Celerity number<br>$\lambda = c_0 / c$                                      |
| Dimensionless river discharge<br>$\varphi = U_r / v$   | Phase lag<br>$\varepsilon = \pi / 2 - (\phi_Z - \phi_U)$                    |

221

222 In this study, we used the analytical solutions proposed by Cai et al. (2014a, b, 2016),  
223 in which the solutions of the major tide-river dynamics are derived by solving a set of  
224 four implicit equations for the tidal damping, the velocity amplitude, the wave celerity,  
225 and the phase lag (see details in Appendix B). The major dependent parameters can be  
226 described by the following four variables (see also Table 1):  $\delta$  represents the  
227 damping/amplification number describing the increase ( $\delta > 0$ ), or decrease ( $\delta < 0$ ) of  
228 the tidal wave amplitude along the estuary axis,  $\mu$  represents the velocity number  
229 indicating the ratio of actual velocity amplitude to the frictionless value in a prismatic  
230 channel,  $\lambda$  represents the celerity number representing the classical wave celerity  $c_0$   
231 scaled by the actual wave celerity  $c$ , and  $\varepsilon$  represents the phase lag between the high  
232 water (HW) and high water slack (HWS) or between the low water (LW) and low water  
233 slack (LWS). It is important to note that the phase lag (ranging between 0 and  $\pi/2$ ) is a  
234 key parameter in classifying the estuary, where  $\varepsilon = 0$  suggests the tidal wave is featured  
235 by a standing wave, while  $\varepsilon = \pi/2$  indicates a progressive wave. For a simple harmonic  
236 wave, the phase lag is defined as  $\varepsilon = \pi/2 - (\phi_z - \phi_U)$ , where  $\phi_z$  and  $\phi_U$  are the phases  
237 of elevation and current, respectively (Savenije, et al., 2008).

238

### 239 **3.2.3 Analytical solution for the entire channel**

240 It is worth noting that the analytically computed tide-river dynamics  $\mu$ ,  $\delta$ ,  $\lambda$ , and  $\varepsilon$  only  
241 represent local hydrodynamics since they depend on local (fixed position) values of the  
242 dimensionless parameters, i.e. the tidal amplitude  $\zeta$ , the estuary shape number  $\gamma$ , the  
243 friction number  $\chi$ , and the river discharge  $\varphi$  (see Table 1). To correctly reproduce the

244 tide-river dynamics for the entire channel, a multi-reach technique is adopted by  
245 subdividing the entire estuary into multiple reaches to account for the longitudinal  
246 variations of the estuarine sections (e.g. bed elevation, bottom friction). For a given  
247 tidal damping/amplification number  $\delta$  and tidal amplitude  $\eta$  at the seaward boundary, it  
248 is possible to determine the tidal amplitude at a distance  $\Delta x$  (e.g. 1 km) upstream by  
249 simple explicit integration. Hence, the analytical solution for the entire channel can be  
250 obtained by step-wise integration in this way.

251

## 252 **4. Results**

### 253 **4.1 Observational analysis on the alteration of tide-river dynamics after TGD** 254 **closure**

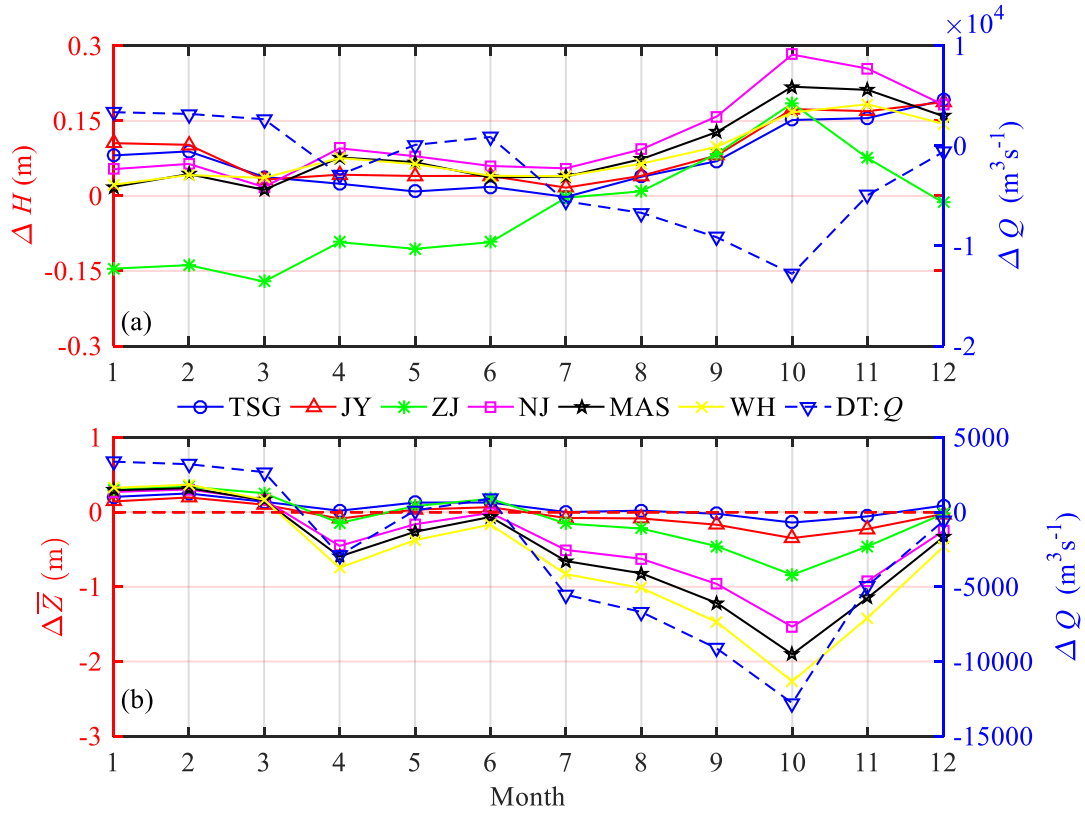
255 To quantify the impacts of TGD operation on the downstream tide-river dynamics, we  
256 divided the time series into two periods, including a pre-TGD period (1979–1984,  
257 representing the condition before the operation of the TGD) and a post-TGD period  
258 (2003–2014, after the closure of the TGD with an operating TGD). Figure 2 shows the  
259 changes in the observed tidal range  $\Delta H$  and residual water level  $\Delta \bar{Z}$  before and after  
260 the closure of the TGD at the six gauging stations, together with the change in  
261 freshwater discharge  $\Delta Q$  observed at the DT hydrological station. Figure 2 and Table 2  
262 clearly show that the monthly averaged river discharge in January, February, and March  
263 substantially increased by 35.5%, 30.5%, and 16.4%, respectively, due to the  
264 considerable release of freshwater from the TGD. On the other hand, we observe a  
265 significant decrease in freshwater discharge in September, October, and November,

266 decreasing by 20.1%, 33.2%, and 20.8%, respectively. The reason can be primarily  
267 attributed to the impounding water of the TGD during these months, especially in  
268 October. During the other months, the impacts of TGD on the change in the freshwater  
269 discharge are relatively small, mimicking the natural condition before the operation of  
270 the TGD.

271

272 In Figure 2a we observe an increasing trend in tidal range for the post-TGD period at  
273 the six gauging stations, except for the marked decrease at the ZJ station in the first half  
274 of the year (i.e. January–June). On average, the maximum increase (0.20 m) in tidal  
275 range occurs in October, which is mainly due to the substantial reduction of river  
276 discharge caused by the TGD operation. This indicates a consistent enhancement of  
277 tidal dynamics along the Yangtze estuary, except the reach near the ZJ station. The  
278 exceptional case in ZJ station is likely due to the fact that ZJ station is located near the  
279 position of the tidal current limit during the dry season (Guo et al., 2015; Zhang et al.,  
280 2018). The shallow and narrow geometry around ZJ station impedes the tidal wave  
281 propagation when river discharge increases due to the TGD operation during the dry  
282 season (Chen et al., 2012), leading to a remarkably decreasing tidal range in the first  
283 half of the year. For the residual water level, Figure 2b clearly shows that the change in  
284 the residual water level directly follows that of the river discharge due to the stable  
285 relationship between these two parameters. In particular, we see that the residual water  
286 levels increased by 0.26 m, 0.30 m, and 0.16 m, respectively, in January, February, and  
287 March, while they significantly decreased by 0.72 m, 1.17 m, and 0.70 m, respectively,

288 in September, October, and November. In addition, the decrease trend in residual water  
 289 level is more significant at upstream stations when compared with those in the  
 290 downstream areas.



291  
 292 Figure 2. Changes in monthly averaged (a) tidal range  $\Delta H$  and (b) residual water level  
 293  $\Delta \bar{Z}$  together with the freshwater discharge  $\Delta Q$  along the Yangtze River estuary.

294  
 295  
 296  
 297  
 298  
 299  
 300

301 Table 2. Comparison of multi-year monthly averaged river discharge  $Q$  ( $\text{m}^3 \cdot \text{s}^{-1}$ )  
 302 between the pre-TGD and the post-TGD periods

| Month    | 1     | 2     | 3     | 4     | 5     | 6     | 7     | 8     | 9     | 10     | 11    | 12    |
|----------|-------|-------|-------|-------|-------|-------|-------|-------|-------|--------|-------|-------|
| Pre-TGD  | 9520  | 10527 | 16298 | 25050 | 30867 | 38283 | 49900 | 47276 | 45317 | 38467  | 23633 | 14810 |
| Post-TGD | 12896 | 13733 | 18974 | 22165 | 30971 | 39180 | 44367 | 40590 | 36187 | 25682  | 18714 | 14203 |
| Change   | 3376  | 3206  | 2675  | -2885 | 105   | 896   | -5533 | -6687 | -9130 | -12784 | -4919 | -607  |

303 Since the TGD operation affects tide-river dynamics primarily through the alteration of  
 304 the freshwater discharge, it is worth exploring the patterns of trends in the relationship  
 305 between the freshwater discharge and gradients of the main tidal parameters with  
 306 respect to distance (i.e. the tidal damping rate and the residual water level slope). Here,  
 307 we estimated the tidal damping rate  $\delta_H$  and the residual water level slope  $S$  for a reach  
 308 of  $\Delta x$  by using the following expressions:

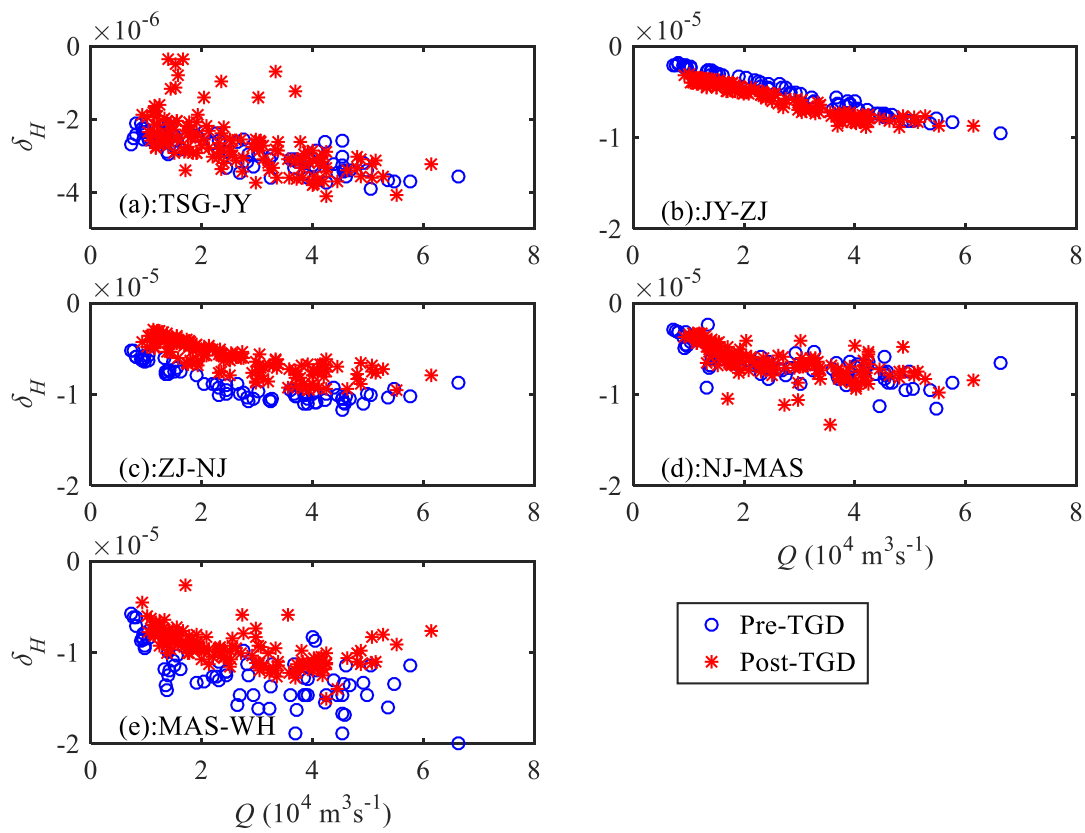
$$309 \quad \delta_H = \frac{1}{(H_1 + H_2)/2} \frac{H_2 - H_1}{\Delta x}, \quad (6)$$

$$310 \quad S = \frac{\bar{Z}_2 - \bar{Z}_1}{\Delta x}, \quad (7)$$

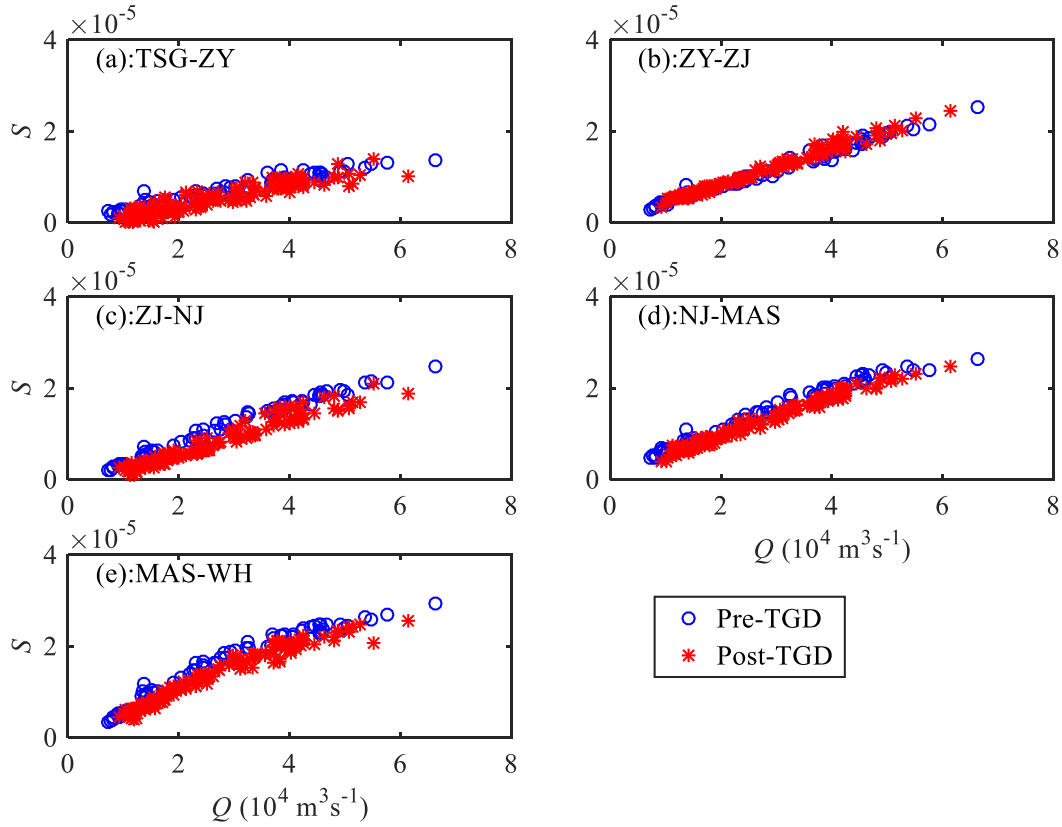
311 where  $H_1$  and  $\bar{Z}_1$  are the tidal amplitude and residual water level on the seaward side,  
 312 respectively, whereas  $H_2$  and  $\bar{Z}_2$  are the corresponding values  $\Delta x$  upstream,  
 313 respectively. Figure 3 presents the computed tidal damping rates for different reaches  
 314 along the Yangtze estuary based on the observed tidal ranges at the six gauging stations.  
 315 It is remarkable that the tidal damping rates at the ZJ-NJ and MAS-WH reaches have  
 316 significantly increased during the post-TGD period, which suggests an enhancement of  
 317 tidal dynamics under the current freshwater discharge conditions. On the contrary, a  
 318 noticeable decrease in  $\delta_H$  was observed at the JY-ZJ reach, which corresponds to a



319 decrease in tidal range at the ZJ station for the low river discharge conditions (from  
 320 January to May, see Figure 2a). At TGS-JY and NJ-MAS, no significant change in  $\delta_H$   
 321 is observed. In Figure 4, a consistent decrease in the residual water level slope  $S$   
 322 observed along the Yangtze estuary, except for the JY-ZJ reach. This means that the  
 323 residual friction effect becomes weaker in the post-TGD period since the residual water  
 324 level slope is primarily balanced by the residual friction term (Cai et al., 2014a, b, 2016).



325  
 326 Figure 3. Changes in tidal damping rate  $\delta_H$  before and after the TGD closure for  
 327 different reaches along the Yangtze estuary: (a) TGS-JY, (b) JY-ZJ, (c) ZJ-NJ, (d) NJ-  
 328 MAS, (e) MAS-WH.



329

330 Figure 4. Changes in residual water level slope  $S$  before and after the TGD closure for  
 331 different reaches along the Yangtze estuary: (a) TGS-JY, (b) JY-ZJ, (c) ZJ-NJ, (d) NJ-  
 332 MAS, (e) MAS-WH.

333

#### 334 4.2 Performance of the analytical model reproducing the tide-river dynamics

335 The analytical model presented in Section 3.2 was subsequently applied to the Yangtze  
 336 River estuary, with the seaward boundary using the tidal amplitude imposed at the TSG

337 station and the landward boundary using the river discharge imposed at the DT station.

338 The computation length of the estuary is 470 km, covering the entire estuary from TSG  
 339 to DT. The adopted geometric characteristics (including the tidally averaged cross-

340 sectional area, width, and depth) are the same for both pre- and post-TGD periods,

341 which were extracted from a digital elevation model (DEM) using Yangtze River

342 estuary navigation charts surveyed in 2007. The geometric characteristics, calibrated  
343 by fitting the observed values using Equations (4) and (5), are presented in Table 3,  
344 where a relatively large cross-sectional area convergence length ( $a = 151$  km) is evident,  
345 with a relatively small width ( $b = 44$  km), indicating a fast transition from a funnel-  
346 shaped reach to a prismatic reach in terms of width. It is worth noting that the Yangtze  
347 River estuary is characterised by a typical semidiurnal character; thus, a typical  $M_2$  tidal  
348 period (i.e. 12.42 h) was adopted in the analytical model. For the sake of simplification,  
349 we assume that the storage width ratio  $r_S = 1$ . Hence, the only calibrated parameter is  
350 the Manning-Strickler friction coefficient  $K$ . Here, we used two values for  $K$ :  $K = 80$   
351  $m^{1/3} \cdot s^{-1}$  in the tide-dominated region ( $x = 0-32$  km), and a smaller value of  $K = 55$   
352  $m^{1/3} \cdot s^{-1}$  in the river-dominated region ( $x = 52-450$  km). In addition, to avoid sharp jump  
353 in the analytically computed parameters due to the adoption of different friction  
354 coefficients, we adopted a friction coefficient of  $K=80-55$   $m^{1/3}s^{-1}$  (indicating a linear  
355 reduction of the friction coefficient) over the transitional reach ( $x=32-52$  km). The  
356 analytically computed results were compared with the observed tidal amplitudes and  
357 the residual water levels at five gauging stations along the Yangtze estuary (Figure 5).  
358 It can be seen that the overall correspondence between analytical results and  
359 observations is good, with high coefficients of determination ( $R^2 > 0.95$ ), which  
360 suggests the usefulness of the present analytical model for reproducing the tide-river  
361 dynamics, given the gross features of flow characteristics and estuarine geometry.

362

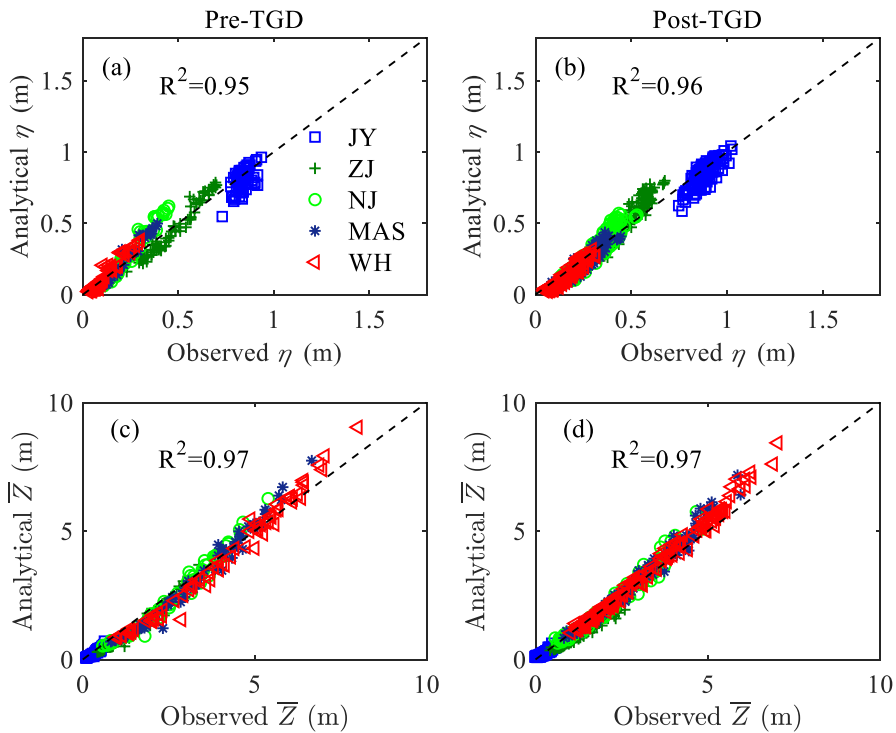
363

364

Table 3. Characteristics of geometric parameters in the Yangtze River estuary

| Characteristics                                  | River  | Mouth  | Convergence length $a/b$ (km) |
|--|--------|--------|-------------------------------|
| Cross-sectional area $\bar{A}$ (m <sup>2</sup> ) | 12,135 | 51,776 | 151                           |
| Width $\bar{B}$ (m)                              | 2005   | 6735   | 44                            |

365



366

367 Figure 5. Comparison of monthly averaged values for (a, b) analytically computed tidal

368 amplitude  $\eta$  and (c, d) residual water level  $\bar{Z}$  against the observations in the Yangtze

369 River estuary for the pre-TGD period (1979–1984) and post-TGD period (2003–2014).

370

371 **4.3 Impacts of TGD operation on spatial-temporal patterns of tide-river dynamics**

372 With the significant seasonal discharge variations resulting from the TGD regulation,

373 an understanding of the seasonal impacts on tide-river dynamics along the estuary has

374 become increasingly important. In Figures 6 and 7, we see how the TGD operation  
375 impacts the longitudinal variation of the main tidal dynamics in terms of the four  
376 dependent parameters  $\delta$ ,  $\lambda$ ,  $\mu$ , and  $\varepsilon$  for different seasons. The most considerable changes  
377 in the major tide-river dynamics occurred in both autumn and winter seasons, which  
378 correspond to the substantial reduction in freshwater discharge in the wet-to-dry  
379 transition period (i.e. autumn) and slightly increased freshwater discharge in the dry  
380 season (i.e. winter) due to the TGD operation since 2003 (see Table 2). On the other  
381 hand, the impacts of the TGD operation on the tide-river dynamics during the spring  
382 and summer are relatively minor due to the negligible change in the freshwater  
383 discharge. However, we do notice that the TGD had exerted slight influence on tide-  
384 river dynamics in the downstream reaches ( $x < 250$  km) during the summer, with the  
385 maximum freshwater discharge occurring within a year. In addition, it appears that there  
386 exists a critical position corresponding to the maximum tidal damping (or minimum  
387 value of  $\delta$ ) upstream in which the tidal damping becomes weak. This phenomenon  
388 occurs particularly in the spring, summer, and autumn. The underlying mechanism is  
389 elaborated in the discussion section.

390

391 Figures 6a, c, e, g show the comparison of the analytically computed tidal damping  
392 number  $\delta$  before and after the closure of the TGD, in which we clearly observe that the  
393 longitudinal tidal damping effect was considerably weakened in autumn, while it was  
394 slightly enhanced in winter after the TGD closure. This was expected since freshwater  
395 discharges tend to dampen the tidal wave primarily through the enhancement of the

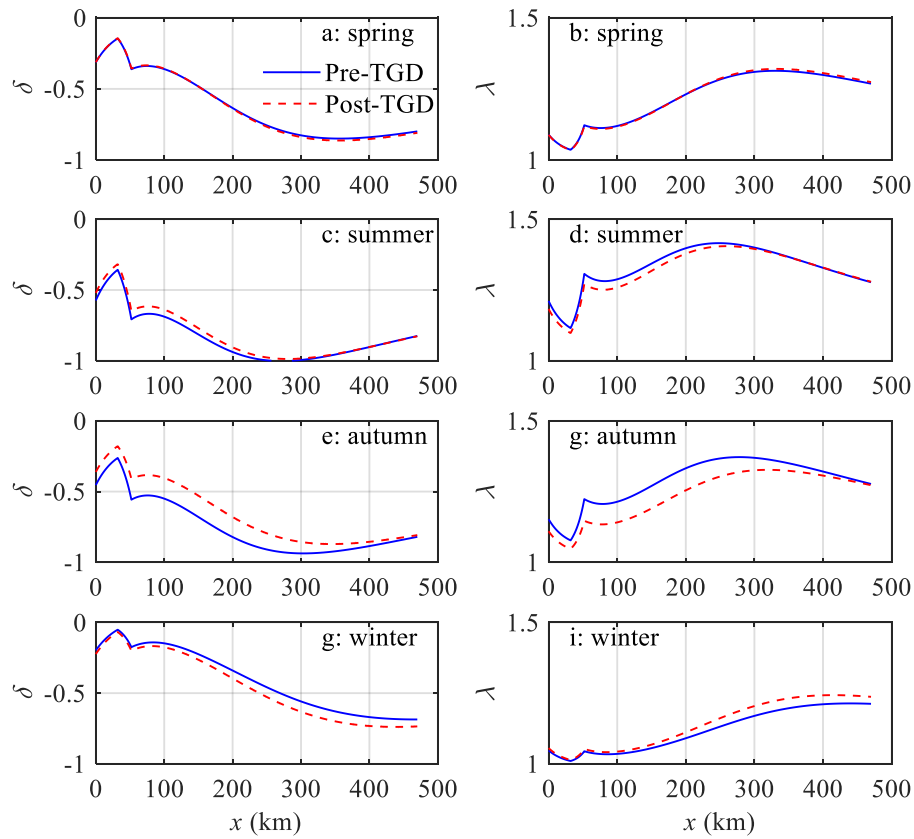
396 friction term (Horrevoets et al., 2004; Cai et al., 2014a, b, 2016). Figures 6b, d, g, i  
397 show a similar picture for the wave celerity number  $\lambda$ , which is positively correlated to  
398 the tidal damping number  $\delta$ , according to the celerity equation (11) in Appendix B.  
399 Figure 7 shows the longitudinal computation of the velocity number  $\mu$  and the phase  
400 lag  $\varepsilon$  for both periods. The impacts of the TGD operation on the velocity scale and phase  
401 lag are similar to the tidal damping, i.e. the larger the freshwater discharge, the smaller  
402 the velocity number and the phase lag. In Figures 6 and 7, there exist switches of the  
403 analytically computed parameters at both ends of the transitional reach ( $x=32-52$  km)  
404 owing to the change in friction coefficient adopted in the analytical model.

405

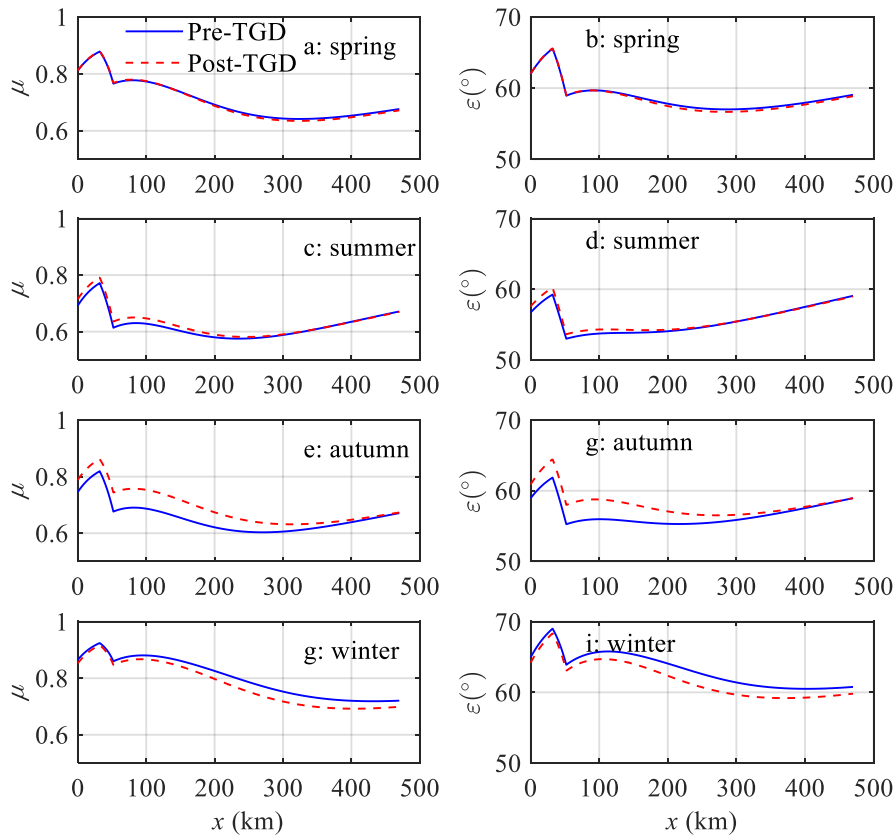
406 Overall, in the seaward reach of the estuary, the effect of freshwater discharge alteration  
407 by the TGD operation on the major tide-river dynamics (i.e.  $\delta$ ,  $\lambda$ ,  $\mu$ , and  $\varepsilon$ ) was less  
408 significant because of the small ratio of freshwater discharge to tidal discharge. On the  
409 other hand, in the upstream reach of the estuary, the changes in the four dependent  
410 parameters are also small due to the substantial tidal attenuation as a result of the long-  
411 distance propagation from the estuary mouth. Therefore, the pattern of seasonal  
412 variation due to the TGD operation is relatively small at both ends of the estuary,  
413 whereas the largest variation usually occurs in the middle reach of the estuary. This  
414 finding was supported by the results of harmonic analysis using the numerical results  
415 (Zhang et al., 2018). Similar phenomena have also been identified in other large fluvial  
416 meso-tide estuaries, such as the Mekong River estuary and Amazon River estuary,  
417 where dam operation altered the seasonal patterns of tide-river dynamics (Kosuth et al.,

418 2009; Hecht et al., 2018).

419



420 Figure 6. Longitudinal variability of simulated tidal damping number  $\delta$  (a, c, e, g) and  
421 celerity number  $\lambda$  (b, d, g, i) along the Yangtze estuary in different seasons (spring: a,  
422 b; summer: c, d; autumn: e, g; winter: g, i) for both the pre-TGD and the post-TGD  
423 periods.



424

425 Figure 7. Longitudinal variability of simulated velocity number  $\mu$  (a, c, e, g) and phase  
 426 lag  $\varepsilon$  (b, d, g, i) along the Yangtze estuary in different seasons (spring: a, b; summer: c,  
 427 d; autumn: e, g; winter: g, i) for both the pre-TGD and the post-TGD periods.

428

## 429 5. Discussion

### 430 5.1 The impact of channel geometry alteration on tide-river dynamics

431 Dam operations, which dramatically modified downstream flow and sediment regimes,  
 432 are becoming an increasingly important factor controlling the morphological evolution.  
 433 Previous studies show that, as a result of the trapping of sediments by the TGD,  
 434 considerable erosion occurred in the first several hundred km downstream of the TGD,  
 435 considerably coarsening the bedload (Yang et al., 2014). In particular, the river bed



436 immediately downstream was eroded at a rate of 65 Mt/yr in 2001–2002 (Yang et al.,  
437 2014). It was shown by Lyu et al. (2018) that due to a dramatic reduction in the sediment  
438 discharge following the construction of the TGD, a significant change in size, geometry,  
439 and spatial distribution of pool-riffles occurred downstream; however, this adjustment  
440 was limited to the reaches close to the TGD. It should be noted that the bathymetry  
441 adopted in the analytical model is restricted to the estuarine area in 2007, which is only  
442 4 years after the TGD closure in 2003, and it is before the full operation of the TGD  
443 began in 2009. In addition, the TGD is around 1600 km away from the estuary mouth,  
444 and its influence on the estuarine morphology normally has a lag effect of at least 4–5  
445 years, as discussed by Wang et al. (2008). Hence, the adopted geometry has been only  
446 partly altered after the TGD closure. The morphological change of Yangtze Estuary can  
447 be even more profound in recent years due to the continuous and accumulated impact  
448 from the TGD. Further adjustment of morphological change due to the sedimentation  
449 in the TGD could exert a considerable impact on the tide-river dynamics in the estuarine  
450 region (e.g., Du et al., 2018; Shaikh et al., 2018). Further study on the impact of  
451 morphological adjustment on the tide-river dynamics is required in the future.

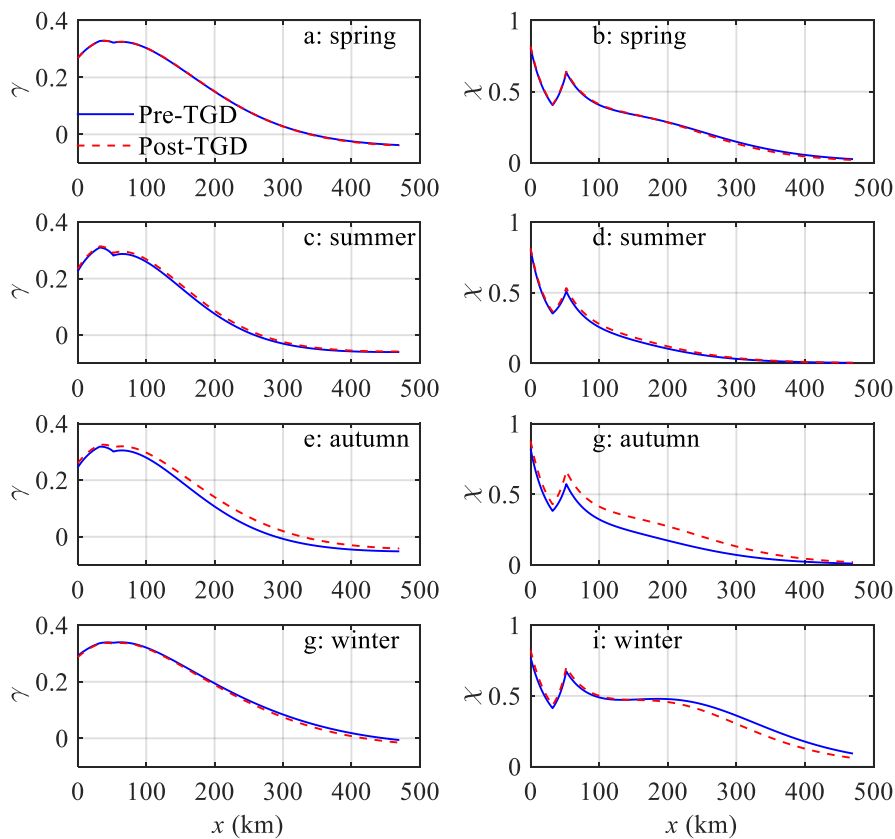
452

## 453 **5.2 The impact of freshwater discharge alteration on tide-river dynamics**

454 The water conservancy of the TGD has multiple purposes, in which the seasonal  
455 discharge regulation and their impact on the ecosystem are well documented (e.g. Mei  
456 et al., 2015a, b; Chen et al., 2016; Guo et al., 2018). However, the actual influence of  
457 discharge regulation on the river-tide dynamics in the estuarine area is not fully

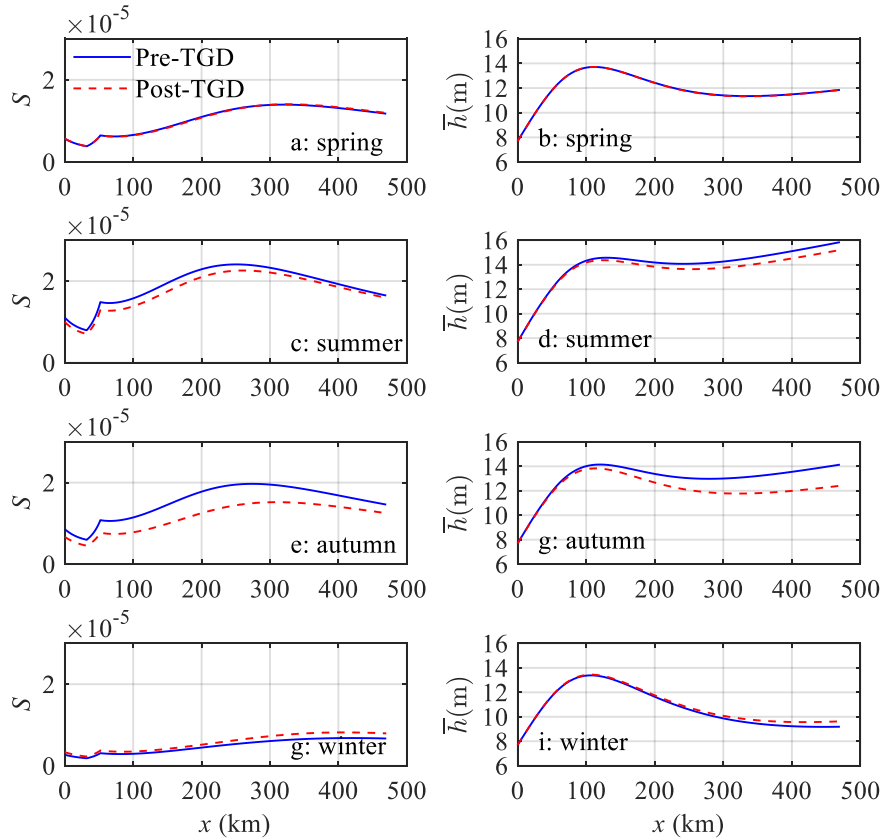
458 understood. With the analytical reproduction of tide-river dynamics for pre- and post-  
 459 TGD periods, it is possible to quantify the extent of the changes in the major tidal  
 460 dynamics, including the estuary shape number  $\gamma$  and friction number  $\chi$  (Figure 8), and  
 461 the residual water level slope  $S$  and water depth  $h$  (Figure 9) along the Yangtze River  
 462 estuary. In general, during the transition from the wet season (summer–autumn) to the  
 463 dry season (winter–spring), the water level and corresponding fluvial discharge  
 464 downstream from the TGD is first raised by the impounding water and then reduced by  
 465 the release of water, which would substantially change the tide-river dynamics in the  
 466 downstream estuarine area, with the maximum variation occurring in autumn and the  
 467 minimum variation occurring in spring.

468



469

470 Figure 8. Longitudinal variability of simulated estuary shape number  $\gamma$  (a, c, e, g) and  
 471 friction number  $\chi$  (b, d, g, i) along the Yangtze estuary in different seasons (spring: a, b;  
 472 summer: c, d; autumn: e, g; winter: g, i) for both the pre-TGD and the post-TGD periods.



473  
 474 Figure 9. Longitudinal variability of simulated residual water level slope  $S$  (a, c, e, g)  
 475 and water depth  $h$  (b, d, g, i) along the Yangtze estuary in different seasons (spring: a,  
 476 b; summer: c, d; autumn: e, g; winter: g, i) for both the pre-TGD and the post-TGD  
 477 periods.

478  
 479 Figures 8 and 9 show that during the wet season (summer–autumn), the estuary shape  
 480 number  $\gamma$  and friction number  $\chi$  experience a general increase, while a decrease in the  
 481 residual water level slope  $S$  and water depth  $\bar{h}$  can be identified in the post-TGD

482 period due to the reduction in freshwater discharge. However, the changes in these  
483 major dynamics vary significantly along the channel. Near the estuary mouth, where  
484 tidal influence overwhelms the influence from freshwater discharge, the difference is  
485 relatively small, as the magnitude of the freshwater discharge is small when compared  
486 with that of the tidal discharge. Meanwhile at the upstream reach of the estuary, where  
487 the riverine influence dominates that of the tide, the difference is also small due to the  
488 attenuation of the tidal wave propagation over a long distance. Consequently, the most  
489 significant changes in major tide-river dynamics occurred in the middle reach of the  
490 Yangtze River estuary due to the discharge regulation of the TGD during the wet season.  
491 By contrast, during the dry season (winter–spring), especially in winter, the opposite  
492 trend was observed, indicating a slight increase in  $\gamma$  and  $\chi$ , and a slight decrease in  $S$   
493 and  $\bar{h}$  due to the additional release of discharge from the TGD. In addition, we also  
494 observed that the changes in tide-river dynamics caused by the TGD operation were  
495 much stronger upstream than in the lower stream.

496

### 497 **5.3 Implications for water resource management**

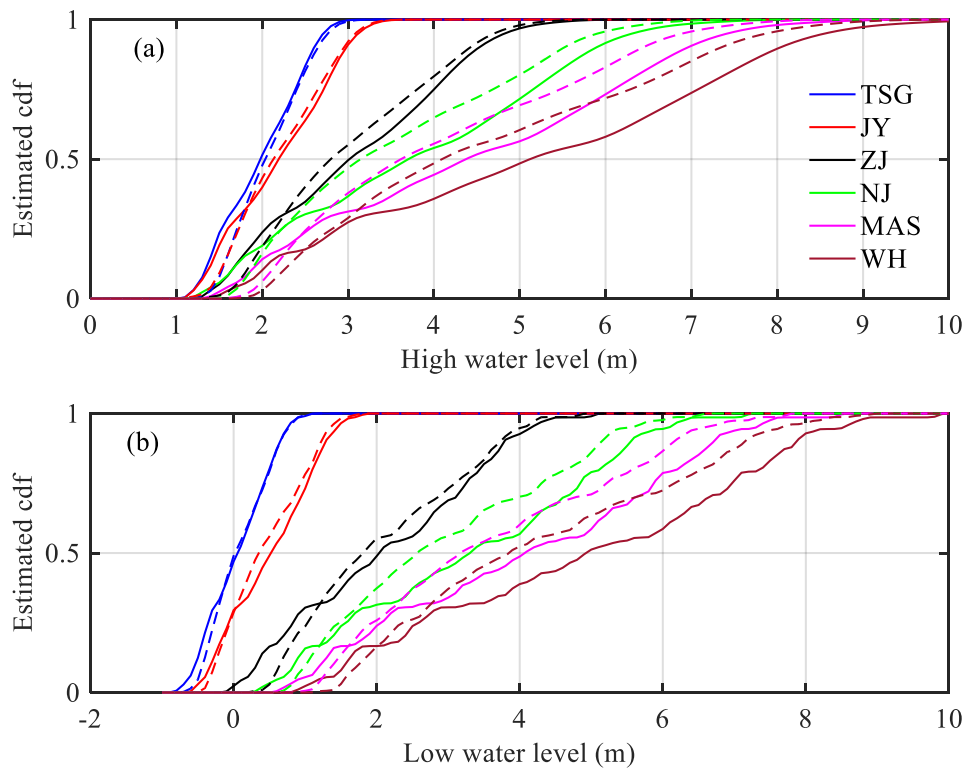
498 The construction of the TGD is the largest hydro-development project ever performed  
499 in the world, having multiple influences on downstream water resource management,  
500 including navigation, flood control, tidal limit variation, and salt intrusion.

501

#### 502 **5.3.1 Implications for navigation**

503 The navigation condition is mainly controlled by both high water and low water levels.

504 Figure 10 shows the estimation of the cumulative distribution function (cdf) for both  
505 the high-water level (Figure 10a) and the low-water level (Figure 10b) at the six  
506 gauging stations along the Yangtze River estuary for both the pre- and post-TGD  
507 periods. The results indicate that navigation conditions during the non-flood season are  
508 generally improved, because both percentages of high-water and low-water levels are  
509 increased due to the additional freshwater discharge released from the TGD. On the  
510 other hand, during the flood season, the reduction in the freshwater discharge by TGD  
511 impounding tends to exert a negative impact on navigation. However, the reduced  
512 freshwater discharges in the late summer and autumn are not of sufficient magnitude to  
513 cause any navigation problems. This is due to the fact that the mean water levels during  
514 the flood season are relatively high; hence, the regulating flow quantity and regulating  
515 capacity are relatively small (e.g. Chen et al., 2016). In general, due to the staggered  
516 regulation in freshwater discharge, seasonally, the actual navigation condition is  
517 improved due to the significant increase in the percentage of low water levels.



518

519 Figure 10. Cumulative distribution function (cdf) estimated by using the kernel  
 520 smoothing function (a) for high water level and (b) low water level at six gauging  
 521 stations along the Yangtze estuary. The solid lines represent the pre-TGD period, while  
 522 the dashed lines represent the post-TGD period.

523

### 524 **5.3.2 Implications for flood control**

525 Flood control is one of the most important functions of building dams and reservoirs in  
 526 large rivers. Before the construction of the TGD, the Yangtze River basin suffered from  
 527 frequent and disastrous flood threats. For instance, the floods of 1998 in the Yangtze  
 528 River were reported to have killed 3656 people, destroyed 5.7 million homes, and  
 529 damaged seven million more. Many studies have examined the flood control capacity  
 530 of the TGD over the past two decades (Zhao et al., 2013; Chen et al., 2014). In particular,  
 531 the capability of the TGD flood control is influenced by multiple factors (e.g. Huang et

532 al., 2018), particularly in the estuarine area, which is strongly influenced by tides from  
533 the ocean. During the flood season, the reduced freshwater discharge by TGD  
534 impounding benefits the flood control by reducing the peak flood discharge. However,  
535 as the tidal influence is enhanced, both the percentages of high water and low water  
536 levels for the post-TGD period are considerably increased, as shown in Figure 10,  
537 indicating a decreased flood control capability. For instance, at the WH gauging station  
538 located in the upstream part of the Yangtze River estuary, the 8-m high-water level  
539 increased by approximately 10% after the TGD closure during the wet season. The  
540 corresponding flood prevention standard, therefore, is reduced due to the increased  
541 high-water level (see also Nakayama and Shankman, 2013).

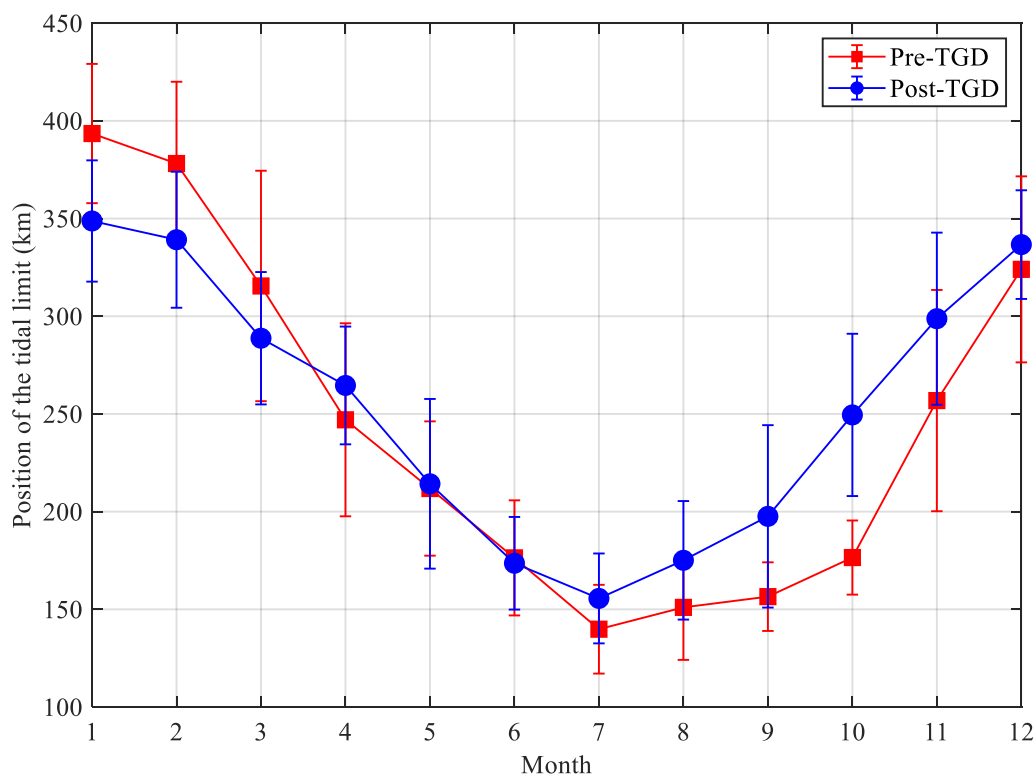
542

### 543 **5.3.3 Implications for tidal limit**

544 It is important to detect the position of the tidal limit (corresponding with the position  
545 where the tidal amplitude to depth ratio is less than a certain threshold, e.g.  $\frac{\eta}{h} < 0.02$ ),  
546 which is the farthest point upstream where a river is affected by tidal fluctuations, since  
547 it is essential for surveying, navigation, and fisheries management, in general (e.g. Shi  
548 et al., 2018). Subsequently, we are able to define the tide-influenced length as the  
549 distance upstream from the estuary mouth to the tidal limit. Generally, the tidal limit  
550 fluctuates with the changes in the seasonal freshwater discharges. Field measurements  
551 have demonstrated that tidal limit can reach as far as the NJ station and further upstream  
552 during the dry season, while during the wet season, it is pushed down to the ZJ station  
553 and may be pushed further downward to the JY station under spate conditions. Figure  
554 11 shows the analytically computed tidal limit position for both the pre- and post-TGD

555 periods. It can be observed that the tidal limit moved downstream by about 45 km and  
 556 39 km in January and February under the impact of the additional release of discharge  
 557 from TGD during the dry season. During the transition from dry to wet seasons  
 558 (January–May), the total freshwater discharge from TGD increases, and we identify  
 559 further downstream movement of the tidal limit, although to a smaller extent. The  
 560 reverse of the post-TGD tidal limit in April is due to the decrease in the freshwater  
 561 discharge compared with the pre-TGD tidal limit (see Table 2). The TGD storage period  
 562 begins in June, and the tidal limit moved upstream by a large amount compared with  
 563 the pre-TGD period. The largest change occurred during October when the tidal limit  
 564 moved from 175 km pre-TGD to 250 km post-TGD due to the substantial increase in  
 565 freshwater discharge (see Table 2).

566



567



568 Figure 11. Temporal variation of the position of the tidal limit relative to the TSG station  
569 for both the pre-TGD and the post-TGD periods. The vertical error bar at each data  
570 point indicates the standard deviation of the analytically computed time series.

571

#### 572 **5.3.4 Implications for salt intrusion**

573 The operation of the TGD changed the location of tidal limit, which, in turn, directly  
574 influences the intensity of saltwater intrusion, especially during the dry season, when  
575 the freshwater discharge is low and saltwater intrusion is important (e.g. Cai et al.,  
576 2015). The analysis of tide-river dynamics shows that the tidal dynamics are  
577 considerably enhanced during the autumn due to the substantial decline in freshwater  
578 discharged into the estuary, which may lead to enhanced saltwater intrusion. However,  
579 with supplemented discharge after the TGD during the winter, saltwater intrusion tends  
580 to be significantly suppressed, and the isohalines are pushed seaward by additional river  
581 discharges (e.g. An et al., 2009; Qiu and Zhu, 2013). In contrast, during the wet season,  
582 the TGD operation slightly extended the timing of saltwater intrusion and increased its  
583 intensity by impounding freshwater. Since the total river discharge rate during the wet  
584 season is the largest during the year, the influence of saltwater on freshwater reservoirs  
585 along the coastal area is limited. Therefore, the operation of TGD is overall favourable  
586 for reducing the burden of freshwater supplement in the tidally influenced estuarine  
587 areas. However, to quantify the potential impacts of TGD's operation on salt intrusion  
588 and related aquatic ecosystem health in general, it is required to couple the  
589 hydrodynamic model to the ecological or salt intrusion model (e.g., Qiu and Zhu, 2013;

590 Cai et al., 2015).

591

## 592 **6. Conclusions**

593 An analytical approach was used to examine the potential impacts of TGD operation  
594 on the spatial-temporal patterns of tide-river dynamics along the Yangtze River estuary.

595 It was shown that the freshwater regulation caused by the TGD, on a seasonal scale,  
596 exerts significant impacts on the tide-river dynamics, with the maximum influence  
597 occurring in autumn and winter. This generally corresponds to a dramatic decrease in  
598 freshwater discharge during the wet-to-dry transition period and a slight increase in  
599 discharge during the dry season. The analytical results indicate that the discharge  
600 regulation by the TGD drives the alterations in the tide-river dynamics instead of the  
601 geometric change. In particular, the change in the freshwater discharge changes the  
602 estuary shape number (representing the geometric effect), the residual water level slope  
603 (representing the effective frictional effect) and, hence, the tide-river dynamics. This  
604 study, using the Yangtze River estuary as an example, provides an effective yet simple  
605 method to quantify the seasonal regulation in freshwater discharge by large reservoirs  
606 or dams on hydrodynamics in estuaries. The results obtained from this study will,  
607 hopefully, shed new light on aspects of water resource management, such as navigation,  
608 flood control, and salt intrusion.

609

610 **Data availability.** Data and results are available from the authors upon request.

611 **Author contributions.** All authors contributed to the design and development of the

612 work. The experiments were originally carried out by Huayang Cai. Xianyi Zhang and  
613 Leicheng Guo carried out the data analysis. Min Zhang built the model and wrote the  
614 paper. Feng Liu and Qingshu Yang reviewed the paper.

615 **Competing interests.** The authors declare that they have no conflict of interest.

616 **Acknowledgments.** We acknowledge the financial support from the National Key  
617 R&D of China (Grant No. 2016YFC0402600), from the Open Research Fund of State  
618 Key Laboratory of Estuarine and Coastal Research (Grant No. SKLEC-KF201809),  
619 from the National Natural Science Foundation of China (Grant No. 51709287 and  
620 41701001), and from the Guangdong Provincial Natural Science Foundation of China  
621 (Grant No. 2017A030310321).

## 622 **References**

623 An, Q., Wu., Y., and Taylor, S.: Influence of the Three Gorges Project on saltwater  
624 intrusion in the Yangtze River Estuary, *Environ. Geol.*, 56, 1679-1686,  
625 <https://doi.org/10.1007/s00254-008-1266-4>, 2009.

626 Alebregtse, N. C., and de Swart, H. E.: Effect of river discharge and geometry on tides  
627 and net water transport in an estuarine network, an idealized model applied to the  
628 Yangtze estuary, *Cont. Shelf. Res.*, 123, 29-49, [https://doi.org/10.1016/](https://doi.org/10.1016/j.csr.2016.03.028)  
629 [j.csr.2016.03.028](https://doi.org/10.1016/j.csr.2016.03.028), 2016.

630 Buschman, F. A., Hoitink, A. J. F., van der Vegt, M., and Hoekstra, P.: Subtidal water  
631 level variation controlled by river flow and tides, *Water Resour. Res.*, 45(10), W10420,  
632 <https://doi.org/10.1029/2009WR008167>, 2009.

633 Cai, H., Savenije, H. H. G., and Toffolon, M.: Linking the river to the estuary, influence

634 of river discharge on tidal damping, *Hydrol. Earth Syst. Sci.*, 18(1), 287-304,  
635 <https://doi.org/10.5194/hess-18-287-2014>, 2014a.

636 Cai, H., Savenije, H. H. G., and Jiang, C.: Analytical approach for predicting fresh water  
637 discharge in an estuary based on tidal water level observations, *Hydrol. Earth Syst. Sci.*,  
638 18(10), 4153-4168, <https://doi.org/10.5194/hess-18-4153-2014>, 2014b.

639 Cai, H., Savenije, H.H.G., Zuo, S., Jiang, C., and Chua, V.: A predictive model for salt  
640 intrusion in estuaries applied to the Yangtze estuary, *J. Hydrol.*, 529, 1336-1349,  
641 <https://doi.org/10.1016/j.jhydrol.2015.08.050>, 2015.

642 Cai, H., Savenije, H. H. G., Jiang, C. Zhao L., Yang Q.: Analytical approach for  
643 determining the mean water level profile in an estuary with substantial fresh water  
644 discharge, *Hydrol. Earth Syst. Sci.*, 20, 1-19, <https://doi.org/10.5194/hess-20-1-2016>,  
645 2016.

646 Chen, J., Finlayson, B.L., Wei, T., Sun, Q., Webber, M., Li, M., and Chen, Z.: Changes  
647 in monthly flows in the Yangtze River, China-With special reference to the Three  
648 Gorges Dam, *J. Hydrol.*, 536, 293-301, <https://doi.org/10.1016/j.jhydrol.2016.03.008>,  
649 2016.

650 Chen, J., Wang, Z., Li, M., Wei, T. and Chen, Z.: Bedform characteristics during falling  
651 flood stage and morphodynamic interpretation of the middle-lower Changjiang  
652 (Yangtze) River channel, China, *Geomorphology*, 147, 18-26,  
653 <https://10.1016/j.geomorph.2011.06.042>, 2012.

654 Chen, J., Zhong, P.A., Zhao, Y.F.: Research on a layered coupling optimal operation  
655 model of the Three Gorges and Gezhouba cascade hydropower stations, *Energy*

656 *Convers. Manage.* 86 (5), 756–763, <https://doi.org/10.1016/j.enconman.2014.06.043>,  
657 2014.

658 Dai, M., Wang, J., Zhang, M., and Chen, X.: Impact of the Three Gorges Project  
659 operation on the water exchange between Dongting Lake and the Yangtze River, *Int. J.*  
660 *Sediment Res.*, 32, 506-514, <https://doi.org/10.1016/j.ijsrc.2017.02.006>, 2017.

661 Dronkers, J. J.: *Tidal Computations in River and Coastal Waters*, Elsevier, New York,  
662 USA, <https://doi.org/10.1126/science.146.3642.390>, 1964.

663 Du, J., Shen, J., Zhang, Y.J., Ye, F., Liu, Z., Wang, Z., Wang, Y.P., Yu, X., Sisson, M.,  
664 Wang, H.V.: Tidal Response to Sea-Level Rise in Different Types of Estuaries: The  
665 Importance of Length, Bathymetry, and Geometry, *Geophys Res Lett.*, 45(1), 227-235,  
666 <https://doi.org/10.1002/2017GL075963>, 2018.

667 Friedrichs, C. T., and Aubrey, D. G.: Non-linear tidal distortion in shallow well-mixed  
668 estuaries, A synthesis, *Estuar. Coast. Shelf S.*, 27, 521-545,  
669 [https://doi.org/10.1016/0272-7714\(88\)90082-0](https://doi.org/10.1016/0272-7714(88)90082-0), 1988.

670 Guo, L., van der Wegen, M., Jay, D.A., Matte, P., Wang, Z.B., Roelvink, D.J.A., He, Q.:  
671 River-tide dynamics, Exploration of nonstationary and nonlinear tidal behavior in the  
672 Yangtze River estuary, *J. Geophys. Res.*, 120(5), 3499-3521,  
673 <https://doi.org/10.1002/2014JC010491>, 2015.

674 Guo, L., Su, N., Zhu, C., and He, Q.: How have the river discharges and sediment loads  
675 changed in the Changjiang River basin downstream of the Three Gorges Dam? *J.*  
676 *Hydrol.*, 560, 259-274, <https://doi.org/10.1016/j.jhydrol.2018.03.035>, 2018.

677 Guo, L., van der Wegen, M., Jay, D.A., Matte, P., Wang, Z.B., Roelvink, D., and He,

678 Q.: River-tide dynamics: Exploration of nonstationary and nonlinear tidal behavior in  
679 the Yangtze River Estuary, *J. Geophys. Res.*, 120(5), 3499-3521,  
680 <https://doi.org/10.1002/2014JC010491>, 2015.

681 Hoitink, A. J. F., and Jay, D. A.: Tidal river dynamics: implications for deltas, *Rev.*  
682 *Geophys.*, 54, 240-272, <https://doi.org/10.1002/2015RG000507>, 2016.

683 Hoitink, A. J. F., Wang, Z. B., Vermeulen, B., Huismans, Y., and Kastner, K.: Tidal  
684 controls on river delta morphology, *Nat. Geosci.*, <https://doi.org/10.1038/ngeo3000>,  
685 2017.

686 Horrevoets, A. C., Savenije, H. H. G., Schuurman, J. N., and Graas, S.: The influence  
687 of river discharge on tidal damping in alluvial estuaries, *J. Hydrol.*, 294, 213-228,  
688 <https://doi.org/10.1016/j.jhydrol.2004.02.012>, 2004.

689 Hecht, J.S., Lacombe, G., Arias, M.E., Duc Dang, T. and Piman, T.: Hydropower dams  
690 of the Mekong River basin, a review of their hydrological impacts, *J. Hydrol.*, 45(10):  
691 W10420, <https://doi.org/10.1016/j.jhydrol.2018.10.045>, 2018.

692 Huang, K., Ye, L., Chen, L., Wang, Q., Dai, L., Zhou, J., Singh, V. P., Huang, M., and  
693 Zhang, J.: Risk analysis of flood control reservoir operation considering multiple  
694 uncertainties, *J. Hydrol.*, 565, 672-684, <https://doi.org/10.1016/j.jhydrol.2018.08.040>,  
695 2018.

696 Kuang, C., Chen, W., Gu, J., Su, T. C., Song, H., Ma, Y., and Dong, Z.: River discharge  
697 contribution to sea-level rise in the Yangtze River Estuary, China, *Cont. Shelf. Res.*,  
698 134, 63-75, <https://doi.org/10.1016/j.csr.2017.01.004>, 2017.

699 Kosuth, P., Callède, J., Laraque, A., Filizola, N., Guyot, J.L., Seyler, P., Fritsch, J.M.,

700 and Guimarães, V.: Sea-tide effects on flows in the lower reaches of the Amazon River,  
701 *Hydrol. Process.*, 23(22), 3141-3150, <https://doi.org/10.1002/hyp.7387>, 2009.

702 Liu, F., Hu, S., Guo, X., Cai, H., Yang, Q.: Recent changes in the sediment regime of  
703 the Pearl River (South China), Causes and implications for the Pearl River Delta,  
704 *Hydrol. Process.*, 32(12): 1771-1785, <https://doi.org/10.1002/hyp.11513>, 2018.

705 Lu, S., Tong, C., Lee, D.Y., Zheng, J., Shen, J., Zhang, W., and Yan, Y.: Propagation  
706 of tidal waves up in Yangtze Estuary during the dry season, *J. Geophys. Res.*, 120(9),  
707 6445-6473, <https://doi.org/10.1002/2014JC010414>, 2015.

708 Lu, X.X., Yang, X., and Li, S.: Dam not sole cause of Chinese drought, *Nature*  
709 475(7355), 174, <https://doi.org/10.1038/475174c>, 2011.

710 Lyu, Y., Zheng, S., Tan, G. and Shu, C.: Effects of Three Gorges Dam operation on  
711 spatial distribution and evolution of channel thalweg in the Yichang-Chenglingji Reach  
712 of the Middle Yangtze River, China, *J. Hydrol.*, 565, 429-442,  
713 <https://doi.org/10.1016/j.jhydrol.2018.08.042>, 2018.

714 Mei, X., Dai, Z., Gelder, P.H.A.J. and Gao, J.: Linking Three Gorges Dam and  
715 downstream hydrological regimes along the Yangtze River, China, *Earth Space Sci.*,  
716 2(4), 94-106, <https://doi.org/10.1002/2014EA000052>, 2015a.

717 Mei, X., Dai, Z., Du, J. and Chen, J.: Linkage between Three Gorges Dam impacts and  
718 the dramatic recessions in China's largest freshwater lake, Poyang Lake, *Sci. Rep.*,  
719 5,18197, <https://doi.org/10.1038/srep18127>, 2015b.

720 Nakayama, T., and Shankman, D.: Impact of the Three-Gorges Dam and water transfer  
721 project on Changjiang floods, *Global Planet Change*, 100, 38-50,

722 <https://doi.org/10.1016/j.gloplacha.2012.10.004>, 2013.

723 Qiu, C. and Zhu., J.: Influence of seasonal runoff regulation by the Three Gorges  
724 Reservoir on saltwater intrusion in the Changjiang River Estuary, *Cont. Shelf Res.*, 71,  
725 16-26, <https://doi.org/10.1016/j.csr.2013.09.024>, 2013.

726 Rahman, M., Dustegir, M., Karim, R., Haque, A., Nicholls, R. J., Darby, S. E.,  
727 Nakagawa, H., Hossain, M., Dunn, F. E., and Akter, M.: Recent sediment flux to the  
728 Ganges-Brahmaputra-Meghna delta system, *Sci. Total Environ.*, 643, 1054-1064,  
729 <https://doi.org/10.1016/j.scitotenv.2018.06.147>, 2018.

730 Räsänen, T. A., Someth, P., Lauri, H., Koponen, J., Sarkkula, J., and Kummu, M.:  
731 Observed river discharge changes due to hydropower operations in the Upper Mekong  
732 Basin, *J. Hydrol.*, 545, 28-41, <https://doi.org/10.1016/j.jhydrol.2016.12.023>, 2017.

733 Sassi, M. G., and Hoitink, A. J. F.: River flow controls on tides and tide-mean water  
734 level profiles in a tidal freshwater river, *J. Geophys. Res.*, 118(9), 4139-4151,  
735 <https://doi.org/10.1002/jgrc.20297>, 2013.

736 Savenije, H. H. G.: *Salinity and Tides in Alluvial Estuaries*, Elsevier, New York, USA,  
737 2005.

738 Savenije, H. H. G.: *Salinity and Tides in Alluvial Estuaries* (2nd completely revised  
739 edition), Available at [www.salinityandtides.com](http://www.salinityandtides.com) (Last access: 10 December 2018),  
740 2012.

741 Savenije, H. H. G., Toffolon, M., Haas, J., and Veling, E. J. M.: Analytical description  
742 of tidal dynamics in convergent estuaries, *J. Geophys. Res.*, 113, C10025,  
743 <https://doi.org/10.1029/2007JC004408>, 2008.



744 Shaikh, B.Y., Bansal, R.K., Das, S.K.: Propagation of Tidal Wave in Coastal Terrains  
745 with Complex Bed Geometry, *Environmental Processes*, 5(3), 519-537,  
746 <https://doi.org/10.1007/s40710-018-0314-7>, 2018.

747 Shi, S., Cheng, H., Xuan, X., Hu, F., Yuan, X., Jiang, Y., and Zhou, Q.: Fluctuations in  
748 the tidal limit of the Yangtze River estuary in the last decade, *Sci. China Earth*  
749 *Sci.*, 61 (8), 1136-1147, <https://doi.org/10.1007/s11430-017-9200-4>, 2018.

750 Wang, Y., Ridd, P.V., Wu, H., Wu, J. and Shen, H.: Long-term morphodynamic  
751 evolution and the equilibrium mechanism of a flood channel in the Yangtze Estuary  
752 (China), *Geomorphology*, 99(1-4), 130-138, [https://doi.org/10.1016/j.geomorph.](https://doi.org/10.1016/j.geomorph.2007.10.003)  
753 [2007.10.003](https://doi.org/10.1016/j.geomorph.2007.10.003), 2008.

754 Vignoli, G., Toffolon, M., and Tubino, M.: Non-linear frictional residual effects on tide  
755 propagation, in, *Proceedings of IAHR Congress*, vol. A, 24-29 August 2003,  
756 Thessaloniki, Greece, 291-298, 2003.

757 Zhang, E. F., Savenije, H. H. G., Chen, S. L., and Mao, X. H.: An analytical solution  
758 for tidal propagation in the Yangtze Estuary, China, *Hydrol. Earth Syst. Sci.*, 16(9),  
759 3327-3339, <https://doi.org/10.5194/hess-16-3327-2012>, 2012.

760 Zhang, F., Sun, J., Lin, B., and Huang, G.: Seasonal hydrodynamic interactions between  
761 tidal waves and river flows in the Yangtze Estuary, *J. Marine Syst.*, 186, 17-28,  
762 <https://doi.org/10.1016/j.jmarsys.2018.05.005>, 2018.

763 Zhang, M., Townend, I., Cai, H., and Zhou, Y.: Seasonal variation of tidal prism and  
764 energy in the Changjiang River estuary: A numerical study, *Chin. J. Oceanol. Limn.*,  
765 34 (1), 219-230, <https://doi.org/10.1007/s00343-015-4302-8>, 2015a.

766 Zhang, M., Townend, I., Cai, H., and Zhou, Y.: Seasonal variation of river and tide  
 767 energy in the Yangtze estuary, China, *Earth Surf. Proc. Land.*, 41(1): 98-116,  
 768 <https://doi.org/10.1002/esp.3790>, 2015b.

769 Zhao, T., Zhao, J., Yang, D. and Wang, H.: Generalized martingale model of the  
 770 uncertainty evolution of streamflow forecasts, *Adv. Water Resour.*, 57, 41-51,  
 771 <https://doi.org/10.1016/j.advwatres.2013.03.008>, 2013.

772

### 773 **Appendix A. Simplified momentum balance for the residual water level slope**

774 Assuming a periodic variation of flow velocity, the integration of Equation (1) over a  
 775 tidal cycle leads to an expression for the residual water level slope (e.g. Cai et al., 2014a,  
 776 2016):

$$777 \quad \frac{\partial \bar{Z}}{\partial x} = -\frac{1}{K^2} \left( \frac{\overline{U|U|}}{h^{4/3}} \right) - \frac{1}{2g} \frac{\partial \overline{U^2}}{\partial x} - \frac{1}{2\rho_0} h \frac{\partial \bar{\rho}}{\partial x} \quad (8)$$

778 where the overbars and the subscript 0 indicate the tidal average and value at the  
 779 seaward boundary, respectively. The residual water level slope is induced by three  
 780 contributions: residual frictional, advective acceleration, and density effects, which  
 781 correspond to the three terms on the right-hand side of Equation (8). Note that the  
 782 contribution from advective acceleration to the residual water level slope:

$$783 \quad \frac{\partial \bar{Z}_{adv}}{\partial x} = -\frac{1}{2g} \frac{\partial \overline{U^2}}{\partial x}, \quad (9)$$

784 can be easily integrated to:

$$785 \quad \bar{Z}_{adv} = -\frac{1}{2g} \left( \overline{U^2} - U_0^2 \right) = -\frac{1}{2} Fr_0 \left( \frac{\overline{U^2}}{U_0^2} - 1 \right) \bar{h}_0 \quad (10)$$

786 where the Froude number is introduced,  $\overline{Fr^2} = \overline{U^2}/(g\bar{h})$ , which is computed with the

787 averaged variables. In this case, the correction is local (not cumulative) and  
 788 proportional to the flow depth through a coefficient that is negligible as long as the  
 789 velocity does not change significantly, and  $Fr$  is small, as is common in most tidal flows.  
 790 It was shown by Savenije (2005, 2012) that the density term in equation (1) always  
 791 exercises a pressure in the landward direction, which is counteracted by a residual water  
 792 level slope, amounting to 1.25% of the estuary depth over the salt intrusion length. The  
 793 value for the residual water level slope, induced by the density effect, is usually small  
 794 compared with the gradient of the free surface elevation; thus, in this paper, we neglect  
 795 the influence of the density difference on the dynamics of the residual water level.

796

## 797 **Appendix B. Governing equations for tide-river dynamics in estuaries**

798 The analytical solutions for the dependent parameters  $\mu$ ,  $\delta$ ,  $\lambda$ , and  $\varepsilon$  are obtained by  
 799 solving the following four dimensionless equations (see details in Cai et al., 2014a):  
 800 the tidal damping/amplification equation, describing the tidal amplification or damping  
 801 as a result of the balance between channel convergence ( $gq$ ) and bottom friction  
 802 ( $cm/G$ ):

$$803 \quad \delta = \frac{\mu^2 (\gamma\theta - \chi\mu\lambda\Gamma)}{1 + \mu^2\beta}, \quad (11)$$

804 the scaling equation, describing how the ratio of velocity amplitude to tidal amplitude  
 805 depends on phase lag and wave celerity:

$$806 \quad \mu = \frac{\sin(\varepsilon)}{\lambda} = \frac{\cos(\varepsilon)}{\gamma - \delta}, \quad (12)$$

807 the celerity equation, describing how the wave celerity depends on the balance between  
 808 convergence and tidal damping/amplification:

809 
$$\lambda^2 = 1 - \delta(\gamma - \delta), \quad (13)$$

810 and the phase lag equation, describing how the phase lag between HW and HWS  
811 depends on wave celerity, convergence, and damping:

812 
$$\tan(\varepsilon) = \frac{\lambda}{\gamma - \delta}, \quad (14)$$

813 where  $q$ ,  $b$ , and  $G$  account for the effect of river discharge and where:

814 
$$\beta = \theta - r_3 \zeta \varphi / (\mu \lambda), \quad \theta = 1 - (\sqrt{1 + \zeta} - 1) \varphi / (\mu \lambda), \quad \Gamma = \frac{1}{\pi} [p_1 - 2p_2 \varphi + p_3 \varphi^2 (3 + \mu^2 \lambda^2 / \varphi^2)].$$
  
815 
$$(15)$$

816 Note that  $\Gamma$  is a friction factor obtained by using Chebyshev polynomials (Dronkers,  
817 1964) to represent the non-linear friction term in the momentum equation:

818 
$$F = \frac{U |U|}{K^2 \bar{h}^{4/3}} \approx \frac{1}{K^2 \bar{h}^{4/3} \pi} (p_0 v^2 + p_1 v U + p_2 U^2 + p_3 U^3 / v) \quad (16)$$

819 in which  $U$  is the cross-sectional averaged velocity consisting of a steady component  
820  $U_r$ , generated by the fresh water discharge, and a time-dependent component  $U_t$ ,  
821 introduced by the tide:

822 
$$U = U_t - U_r = v \sin(\omega t) - Q / \bar{A} \quad (17)$$

823 where  $Q$  is the fresh water discharge (treated as a constant during the tidal wave  
824 propagation), and  $p_i$  ( $i = 0, 1, 2, 3$ ) are the Chebyshev coefficients (see Dronkers, 1964,  
825 p. 301), which are functions of the dimensionless river discharge  $\varphi$  through  $\alpha = \arccos(-$   
826  $\varphi)$ :

827 
$$p_0 = -\frac{7}{120} \sin(2\alpha) + \frac{1}{24} \sin(6\alpha) - \frac{1}{60} \sin(8\alpha), \quad (18)$$

828 
$$p_1 = \frac{7}{6} \sin(\alpha) - \frac{7}{30} \sin(3\alpha) - \frac{7}{30} \sin(5\alpha) + \frac{1}{10} \sin(7\alpha), \quad (19)$$

829 
$$p_2 = \pi - 2\alpha + \frac{1}{3} \sin(2\alpha) + \frac{19}{30} \sin(4\alpha) - \frac{1}{5} \sin(6\alpha), \quad (20)$$

830 
$$p_3 = \frac{4}{3} \sin(\alpha) - \frac{2}{3} \sin(3\alpha) + \frac{2}{15} \sin(5\alpha). \quad (21)$$

831 The coefficients  $p_1$ ,  $p_2$ , and  $p_3$  determine the magnitudes of the linear, quadratic, and

832 cubic frictional interaction, respectively.

833